Density-functional theory study on the electronic properties of laves phase superconductor $CaIr_2$*

Yi Zhang(张奕), Xiang-Ming Tao(陶向明), and Ming-Qiu Tan(谭明秋)†

Department of Physics, Zhejiang University, Hangzhou 310027, *China*

(Received 3 November 2016; revised manuscript received 19 January 2017; published online 10 March 2017)

In this work we have used density-functional theory methods such as full-potential local orbital minimum basis (FPLO) and ELK-flapw to study the electronic structure of newly discovered Laves phase superconductor $CaIr_2$. The calculation of density of states (DOS) indicates that the bands near Fermi level are mostly occupied by the d-electrons of iridium. The simulation of de Haas–van Alphen (dHvA) effect has been performed by using Elk code to check the Fermi surface topology. The results show that there exist four Fermi surfaces in $CaIr_2$, including two electron-type and two hole-type surfaces. The optical response properties of $CaIr_2$ have been calculated in the dipole-transition approximations combined with including intra-band Drude-like terms. In the optical spectrum $\sigma(\omega)$ shows that the crossover from intra-band to inter-band absorption occur near 1.45 eV. Further analysis on the electron energy loss spectra (EELS) matches the conclusion from that of optical conductivity $\sigma(\omega)$.

Keywords: electronic structure, optical properties, density-functional calculation

PACS: 74.25.Jb, 78.20.Ci **DOI:** 10.1088/1674-1056/26/4/047401

1. Introduction

For the past few years, it has been reported that spin–orbit interaction plays an important role in determining the electronic properties of metallic compounds, especially those that contain f-electrons, which sometimes causes the time-reversal-invariant topological insulators or superconductors.[1–9] Iridium oxides with the pyrochlore lattice have been predicted to have extraordinary electronic properties and behaviors like metal-insulator transition.[10,11] In addition to this work, Neel Haldolaarachchige *et al.*[12] found that the Laves phase[12–14] compound $CaIr_2$ is a superconductor of $T_c \sim 5.8$ K which was considered as 4 K∼6.2 K in the past.[15–18] That paper also presented a band-structure calculation combined with the discussions on the effect of the spin–orbit coupling by using Wien2k,[19–21] hypothesizing the superconductivity might be the result of the pyrochlore lattice of heavy metal atom iridium. The Fermi surfaces in this compound have been calculated in both scalar relativistic and fully relativistic cases.

Frankly the band-structure calculation in Ref. [12] could not be viewed as a complete one. We have evaluated the electronic structure by different codes and found that the topology of Fermi surfaces in Ref. [12] is actually problematic. In order to get more detailed insights for this material, we present our first-principle calculation on $CaIr_2$ by density-functional based on FPLO code[22] and Elk code.[23] As for the topology of Fermi surfaces, this study really yields somewhat different pictures. Furthermore we perform an optical calculation based on the density-functional theory which might provide theoretical reflection spectrum and optical conductivity spectrum. The authors believe that these data may be used as references for experiments.

This paper is organized as follows: In Section 2, the structural model of $CaIr_2$ and computational methods used in this study have been described and presented; In Section 3 the calculation results have been extensively described and discussed including band structures, Fermi surface topology, dHvA effects, and optical properties; In the final section, Section 4, the essential results and conclusions are summarized.

2. Structural model and computational method

The space group of Laves phase $CaIr_2$ is Fd-3m (No. 227) and the corresponding experimental lattice parameters, i.e., $a = 7.545$ Å have been reported in an earlier paper.[24] This lattice parameter will be used throughout this work. The Ca atoms are located at 8b (3/8, 3/8, 3/8) site and Ir are located at 16c (0, 0, 0). Each face of the cubic cell contains 5 Ir atoms along the diagonal and the remaining six ones form a hexagon inside the body. They make a centrosymmetric structure with respect to Ca in the unit cell. The calculations of electronic structures are performed by using Perdew–Zunger LSDA exchange[25] and the correlation potential implemented in Elk-flapw and FPLO codes. We also calculated de Haas-van Alphen frequencies.[26] It has been used to detect the Fermi surfaces on experimental work since it appeared.[27–32] However, it can also be considered as an effective simulation method on checking Fermi surface geometry depending

*Project supported by the National Natural Science Foundation of China (Grant No. 11274084).

†Corresponding author. E-mail: mqtan@zju.edu.cn

© 2017 Chinese Physical Society and IOP Publishing Ltd

on the results of band energiesby using the Supercell *K*-space Extremal Area Finder (SKEAF) code which can be downloaded from Ref. [23], also belonging to Elk code. The optics properties are studied and tested by Wien2k and FPLO, based on Kramer–Kronig relation as many other simulation works did.[33–36]

3. Results and discussion

Figure 1 shows the electronic band structure in the scalar relativistic approximation. The area near Fermi energy is filled with d-states of iridium by just examining the band weights. Figure 2 gives the densities of states (DOS) in $CaIr_2$. It shows that despite 3d-state dominants the DOS of Ca, it is still too small in comparison with the 5d-state of Ir. According to the band weight results in Fig. 1, the states near Fermi level are derived by iridium $d_{xy}+d_{z^2}$ electrons. This result is different from Ref. [12] which claims that the states near the Fermi level do not contain d_{z^2} orbit. We obtained the band structure with spin–orbital interaction (SOC) by using FPLO and displayed these figures in Fig. 3. The splitting parts marked with red circles are the same as those in Ref. [12], which leads to the conclusion that the band weights calculated by FPLO are also reliable. The effect of SOC may not be remarkable, for $CaIr_2$ is a centrosymmetric superconductor.[37,38]

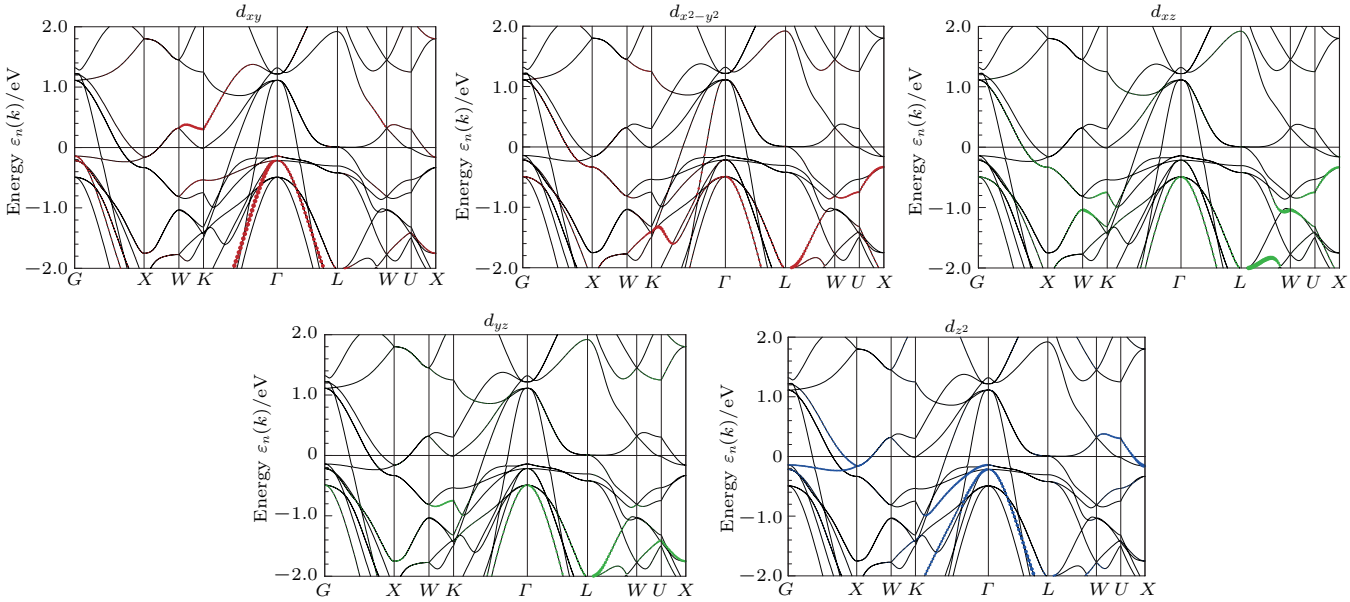


Fig. 1. (color online) The band weight structure of $CaIr_2$. The compositions of states are titled on each top of the picture. The same color represents the atomic orbits with same magnetic quantum number.

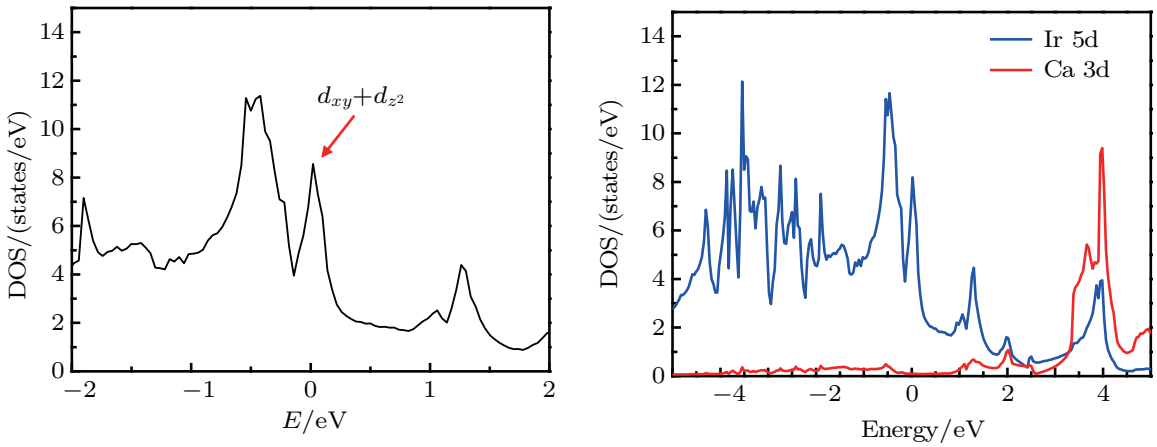


Fig. 2. (color online) The DOS of $CaIr_2$ and a comparison of d electron states without SOI. The compositions of states near the Fermi level are pointed out.

Figure 4 shows the Fermi surfaces of $CaIr_2$ in the *k*-space. We have checked the four Fermi surfaces by both Elk-flapw and FPLO. Finally these two methods yield almost identical results. Then we extracted the de Haas–van Alphen data from the analysis on Fermi surfaces and demonstrated the comparison results in Figs. 5 and 6. The simulation is based on the correlation between dHvA frequency and extremal area of Fermi surface.[39] As the frequency is a function of magnetic induc-

tion strength, the figures of dHvA frequencies use 1000 T as the unit of vertical axis. We determined scanned area by fixing the direction parallel with the xy plane and rotating it from x axis to y axis. The angle from x axis to y axis is noted as θ. These four surfaces correspond to the four bands across the Fermi level from the highest energy to the lowest energy. All of them are symmetrical that measure up with the geometry structure of $CaIr_2$. The first surface is an irregular sphere. If the shape is a perfect sphere, the dHvA results should be a horizontal line because every direction of magnetic field will get the same cross-area of the Fermi surface.[39] The line becomes not flat when the curvature changes, just like the black line's behavior in Fig. 6(a). The second surface is a much larger sphere with breaches resembling a "chimney" along [111] direction. The chimneys seem to be open in the picture as the gradient rises rapidly to infinity, which implies that the Fermi surface is connected in k-space.[39] The small peaks near 30° and 60° are caused by that unsmooth surface. The curve near 45° is divergent which can be caused only by open structures. Comparing to the results in Ref. [12], the mouths of the chimneys are much smaller in our work.

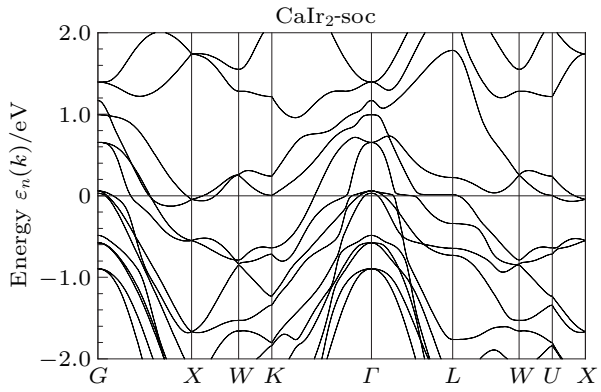


Fig. 3. The band structure of $CaIr_2$ with SOC from FPLO method.

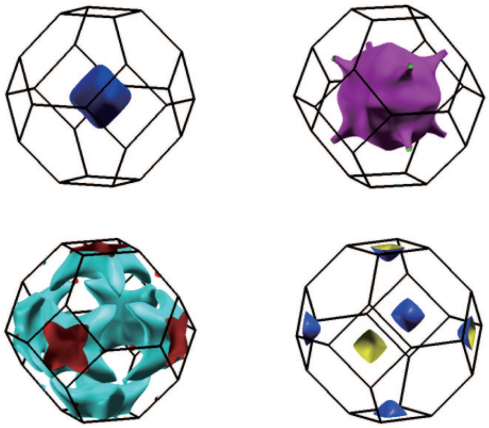


Fig. 4. (color online) The four Fermi surfaces calculated by Elk and drawn by XCrySDen.[16] Panels (a)–(d) correspond to the bands which are ordered from the highest energy to the lowest energy.

It is clear in Fig. 7(e) that the section of this chimney is a just size through the area formed by the sharp corners of the third surface. The third Fermi surface is complex at first glance, but no differences in topological properties from the others. Three nearby surfaces give sharp angles on the plane (111) and these curious shells wrap up the last surface. The last Fermi surface resembles a cube with curvy surfaces. In fact their skins are not smooth. We present the detailed dHvA results with more scanned angles in Fig. 6(d) where the line becomes jagged. The results calculated by FPLO in Fig. 7 are the same with Elk results, which lead us to believe that both Elk and FPLO Fermi surfaces yield the same and correct Fermi surface topology. According to the FPLO images, the first two bands contribute to hole-type carriers and the rest two yield electron-type carriers.

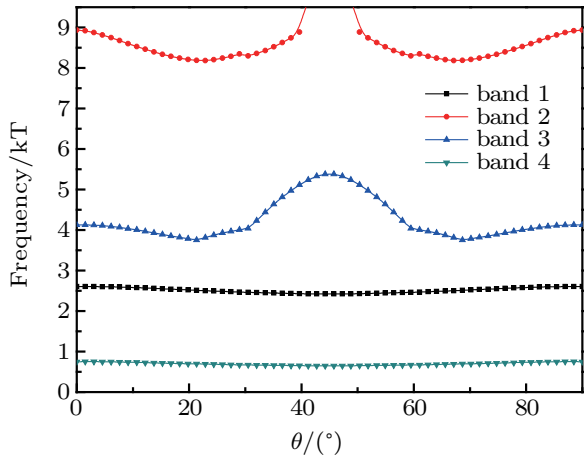


Fig. 5. (color online) The de Haas–van Alphen simulation results. The four surfaces are drawn in one picture for a comparison. The scales of frequencies are associated with the volume of Fermi surfaces.

Figure 8 gives the optical properties of $CaIr_2$ calculated by Wien2k.[40,41] The picture of $\sigma(\omega)$ shows that the optical conductivity decreases before 0.8 eV, suggesting the main absorption to be intraband type, which is also confirmed in the results from FPLO. As the photon energy increases, more electrons can be stimulated from valence bands to conduction bands. The peak of inter-band absorption appears at about 1.45 eV. In the energy range above 3.2 eV, the conductivity becomes relatively flat because the motivations disappear. Actually these observations support the corresponding calculated band structures well. The energy gaps between valence bands and conduction bands at high-symmetry points in Bouillon zone are about 1.4 eV which can achieved from Fig. 1.

The electron energy loss spectra (EELS) in Fig. 8 shows that the loss of energy increases with the photon energy. We performed the electronic conductivity and energy loss spectra with energy range from 0 eV to 30 eV and the detailed part from 0 eV to 5 eV of EELS. There are obviously small peaks at 0.8 eV and they sunken near 1.4 eV, which matches the analysis on electronic conductivity in such a range. According to

the description of electronic conductivity and energy loss function, there is a district reciprocal relation between them, which can be viewed from the figures qualitatively.

$$\mathrm{Re}\,\sigma(\omega) = \frac{1}{4\pi}\omega\,\mathrm{Im}\,\varepsilon(\omega),$$

$$L = -\mathrm{Im}\left(\frac{1}{\varepsilon(\omega)}\right),$$

where $\mathrm{Re}\,\sigma(\omega)$ is the real part of electronic conductivity function. $\mathrm{Im}\,\varepsilon(\omega)$ is the imaginary part of dielectric function. L is the energy loss function.

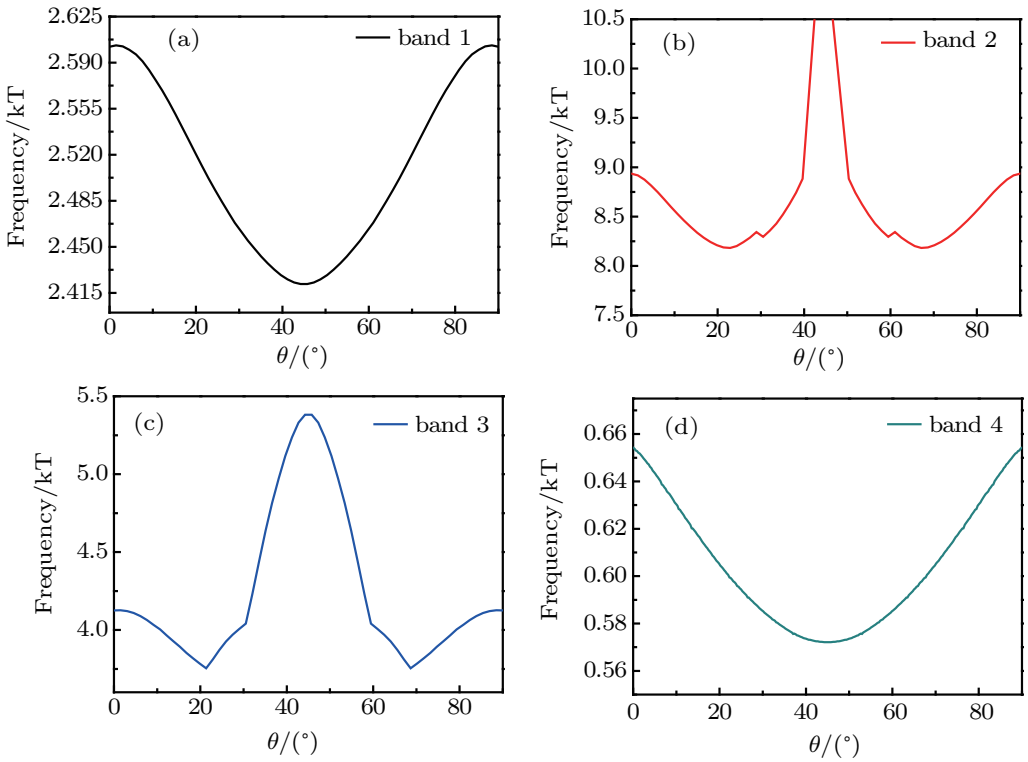


Fig. 6. (color online) The four surfaces are drawn separately for their detailed properties. It can be seen that the line in panel (d) is not that smooth compared to that in panel (a), although they reflect to similar shapes of the Fermi surface.

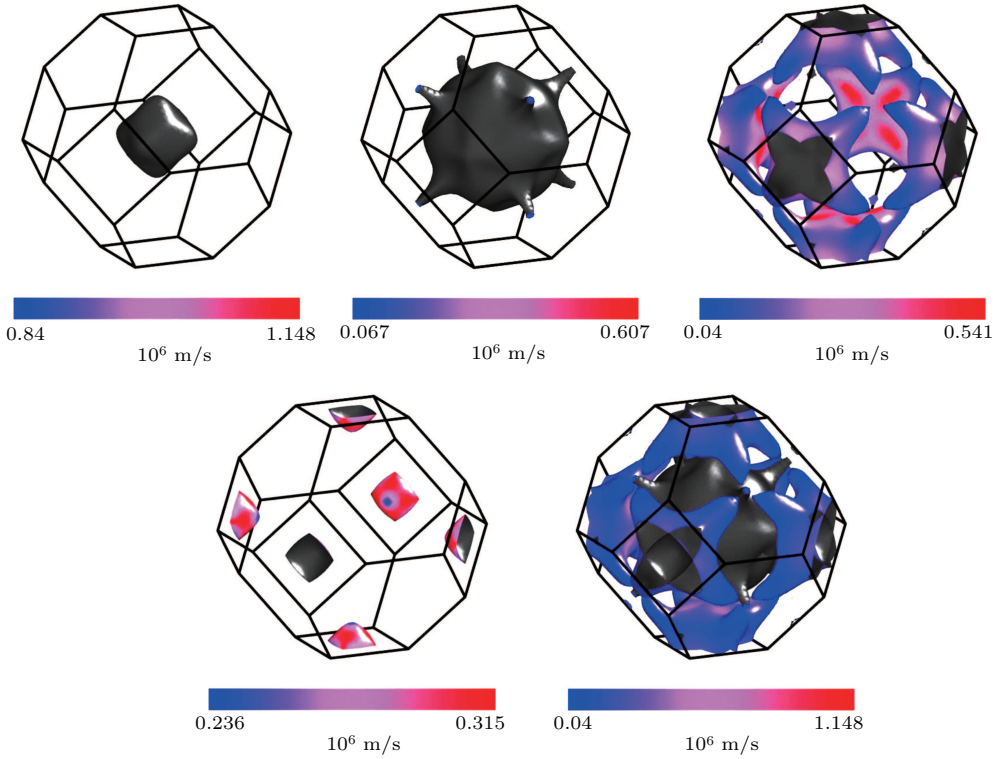


Fig. 7. (color online) The Fermi surfaces calculated by FPLO. The grey side goes to hole-type carriers and colorized side goes to electron-type carriers. The scales at bottom of each picture are for the Fermi velocity.

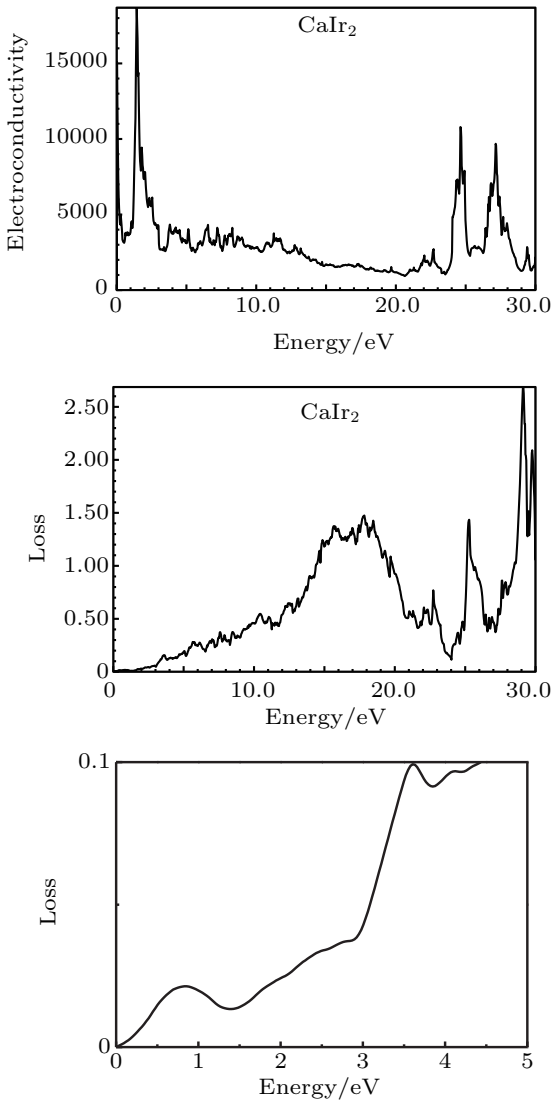


Fig. 8. The optical conductivity spectra and EELS calculated by Wien2k.

The energy loss spectrum physically shows how the energy is absorbed when electron moves across the solid, so the expression of EELS can fit the reflection spectrum well on each peak and valley.[42,43] That is why we did not display the reflection spectrum. The flat part from 10 eV to 20 eV which seems to contain lots of peaks can be viewed as the combination of excitation loss peaks of valence electrons and plasma elementary loss peaks. The peaks at 25.5 eV and 29.3 eV and the valleys between them correspond to the opposite shapes in conductivity spectrum at the same energy. They shows the plasma oscillation near the plasma edge.[36] Since the SOC affected the electric structures, the optical properties should also be recalculated. However, the psudopotential under the circumstance of SOC has not been worked out yet, which might give an inaccuracy result of optical properties. That is why we did not perform the results under SOC.

All the results carried out by Wien2k are same as those carried out by FPLO.

4. Conclusion

In summary we have demonstrated the electronic structure and related optical properties of $CaIr_2$ in this work. Specifically the Fermi surfaces and dHvA data have been drawn by using ELK-flapw code in this work firstly. The states near the Fermi surface are mostly 5d-electrons of Ir. Furthermore the $\sigma(\omega)$ and EELS indicates that the main absorption is intra-band type before 0.8 eV and turns to be inter-band type near 1.45 eV. The results calculated by using different methods (FPLO & Wien2k) are the same. A further study on its electron–phonon interaction may reveal more properties and provides insight regarding the origins of superconductivity of this compound. Since now there are few experimental results on $CaIr_2$, we hope that this simulation work can push on some extra-works on it, especially electronic structure scanning and optical properties exploring.

Acknowledgments

The first of authors (Yi Zhang) would like to express his grateful thanks to Mr. Wazir Tariq Usman for his help during the preparation of this manuscript.

References

[1] Fu L, Kane C L and Mele E J 2007 *Phys. Rev. Lett.* **98** 106803
[2] Kane C L and Mele E J 2005 *Phys. Rev. Lett.* **95** 226801
[3] Moore J E and Balents L 2007 *Phys. Rev. B* **75** 121306
[4] Schnyder A P, Ryu S, Furusaki A and Ludwig A W W 2008 *Phys. Rev. B* **78** 195125
[5] Kitaev A 2009 *AIP Conf. Proc.* **1134** 22
[6] Qi X L, Hughes T L, Raghu S and Zhang S C 2009 *Phys. Rev. Lett.* **102** 187001
[7] Hasan M Z and Kane C L 2010 *Rev. Mod. Phys.* **82** 3045
[8] Liang Y, Wu X X and Hu J P 2015 *Chin. Phys. Lett.* **32** 117402
[9] Liu Y, Zhao J Z, Yu L, Lin C T, Liang A J, Hu C, Ding Y, Xu Y, He S L, Zhao L, Liu G D, Dong X L, Zhang J, Chen C T, Xu Z Y, Weng H M, Dai X, Fang Z and Zhou X J 2015 *Chin. Phys. Lett.* **32** 067303
[10] Witczak-Krempa W, Chen G, Kim Y B and Balents L 2014 *Ann. Rev. Condens. Matter Phys.* **05** 57
[11] Yang B J and Kim Y B 2010 *Phys. Rev. B* **82** 085111
[12] Haldolaarachchige N, Gibson Q, Schoop L M, Luo H and Cava R J 2015 *J. Phys: Condens. Matter* **27** 185701
[13] Compton V B and Matthias B T 1959 *Acta Crystallographica* **12** 651
[14] Johannes R L, Haydock R and Heine V 1976 *Phys. Rev. Lett.* **36** 372
[15] Stein F, Palm M and Sauthoff G 2004 *Intermetallics* **12** 713
[16] Matthias B T and Corenzwit E 1957 *Phys. Rev.* **107** 1558
[17] Ku H C, Matthias B T, Barz H 1979 *Solid State Commun.* **32** 937
[18] Takeya H, ElMassalami M, Terrazos L A, Rapp R E, Capaz R B, Fujii H, Takano Y, Doerr M and Granovsky S A 2013 *Sci. Technol. Adv. Mater.* **14** 3
[19] http://www.wien2k.at
[20] Blaha P, Schwarz K, Madsen G K H, Kvasnicka D and Luitz J 2001 WIEN2k, An Augmented Plane Wave + Local Orbitals Program for Calculating Crystal Properties (Techn. Universität Wien, Austria) ISBN 3-9501031-1-2
[21] Blaha P, Schwarz K, Sorantin P and Trickey S B 1990 *Comput. Phys. Commun.* **59** 399
[22] http://www.fplo.de
[23] http://elk.sourceforge.net/
[24] Wood E A and Compton V B 1958 *Acta Crystallographica* **11** 429
[25] Perdew J P and Zunger A 1981 *Phys. Rev. B* **23** 5048

[26] Onsager L 1952 The London, Edinburgh, and Dublin Philosophical Magazine and Journal of Sceince ISSN:1941-5982
[27] McClure J W 1957 *Phys. Rev.* **108** 612
[28] Kohn W 1961 *Phys. Rev.* **123** 1242
[29] Aoki H, Uji S, Albessard A K and Onuki Y 1993 *Phys. Rev. Lett.* **71** 2110
[30] Putzke C, Coldea I, Guillamón I, Vignolles D, McCollam A, LeBoeuf D, Watson M D, Mazin I I, Kasahara S, Terashima T, Shibauchi T, Matsuda Y and Carrington A 2012 *Phys. Rev. Lett.* **108** 047002
[31] Terashima T, Kurita N, Kimata M, Tomita M, Tsuchiya S, Imai M, Sato A, Kihou K, Lee C H, Kito H, Eisaki H, Iyo A, Saito T, Fukazawa H, Kohori Y, Harima H and Uji S 2013 *Phys. Rev. B* **87** 224512
[32] Shoenberg D 1984 *Magnetic Oscillations in Metals* (Cambridge: Cambridge University Press)
[33] Adolph B, Furthmüller J and Bechstedt F 2001 *Phys. Rev. B* **63** 125108
[34] Guo G Y, Wang D S and Duan C G 2004 *Phys. Rev. B* **69** 205416
[35] Mircholi F and Moghadam H G 2015 *Optik-International Journal for Light and Electron Optics* **126** 17
[36] Hu C H, Yin X H, Wang D H, Zhong Y, Zhou H Y and Rao G H 2016 *Chin. Phys. B* **25** 067801
[37] von Rohr F, Luo H, Ni N, Wörle M and Cava R J 2014 *Phys. Rev. B* **89** 224504
[38] Klimczuk T, Ronning F, Sidorov V, Cava R J and Thompson J D 2007 *Phys. Rev. Lett.* **99** 257004
[39] Rouke P M and Julian S R 2012 *Comput. Phys. Commun.* **183** 324
[40] Abt R, Ambrosch-Draxl C and Knoll P 1994 *Physica B* **194–196** 1451
[41] Ambrosch-Draxl C and Sofo J 2006 *Comput. Phys. Commun.* **175** 1
[42] Shang X F, Tao X M, Chen W B, Chen H X, Wang M and Tan M Q 2008 *Acta Phys. Sin.* **57** 5838 (in Chinese)
[43] Liu Q, Cheng X L, Li D H and Yang Z J 2010 *Acta Phys. Sin.* **59** 8829 (in Chinese)